The structure of the KtrAB potassium transporter

Ricardo S. Vieira-Pires1, Andras Szollosi1 & João H. Morais-Cabral1

1IBMC, Instituto de Biologia Molecular e Celular, Universidade do Porto, Rua do Campo Alegre 823, Porto 4150-180, Portugal.

Originally published in Nature 496, 323–328, April 18, 2013.

DOI: 10.1038/nature12055

In bacteria, archaea, fungi and plants the Trk, Ktr and HKT ion transporters are key components of osmotic regulation, pH homeostasis and resistance to drought and high salinity. These ion transporters are functionally diverse: they can function as Na^+ or K^+ channels and possibly as cation/K^+ symporters. They are closely related to potassium channels both at the level of the membrane protein and at the level of the cytosolic regulatory domains. Here we describe the crystal structure of a Ktr K^+ transporter, the KtrAB complex from *Bacillus subtilis*. The structure shows the dimeric membrane protein KtrB assembled with a cytosolic octameric KtrA ring bound to ATP, an activating ligand. A comparison between the structure of KtrAB–ATP and the structures of the isolated full-length KtrA protein with ATP or ADP reveals a ligand-dependent conformational change in the octameric ring, raising new ideas about the mechanism of activation in these transporters.

The Trk/Ktr/HKT superfamily of ion transporters includes the Trk, Ktr and HKT transporter families[1]. These transporters are closely related to the superfamily of tetrameric cation channels[2–4], which includes potassium, sodium and calcium channels. The membrane proteins in both superfamilies share the same architecture[2,5–9]: four subunits or repeats, each with the TM–P loop–TM (where TM indicates transmembrane helix) structural motif first seen in the KcsA potassium channel structure[10], assemble to form an ion pore with a 'selectivity filter' along its central axis. In addition, the cytosolic regulatory proteins of the Trk and Ktr transporters and of the MthK[11,12] and large-conductance Ca^{2+}-gated (BK) K^+ channels[13–15] are RCK (regulate conductance of K+) domains.

Ktr ion transporters are crucial K^+ transport systems in some bacteria[16,17], with a role in resistance to osmotic stress and high salinity by mediating the early uptake of K^+ (refs 16, 18). The Ktr ion transporters are composed of two essential components[3,16]: a membrane protein (KtrB or KtrD) and a cytosolic regulatory protein (KtrA or KtrC). Studies with cells show that Ktr proteins[8,19] transport K^+ but are also permeable to Na^+, and that K^+ transport is ATP[20] and Na^+ dependent[5,8,18]. Furthermore, it has been shown that truncated KtrA forms octameric rings[21,22] and that KtrB assembles as homodimers[6,21]. The structures described here clarify the molecular basis of some of these properties as well as the structural relationship between these transporters and ion channels.

KtrAB architecture

We have determined the structure of a KtrAB potassium transporter with diffraction data to 3.5 Å (Fig. 1 and Supplementary Table 1). Two diffraction data sets to better than 4 Å were collected out of many thousands of crystals tested. The structure was determined from an anisotropic diffraction data set which extends to 3.3 Å in the best direction; four- and eight-fold averaging together with cross-crystal averaging led to the calculation of high-quality electron-density maps (Supplementary Fig. 1). The crystallographic asymmetric unit contains a KtrA octameric ring associated with two identical KtrB dimers, one on each face of the ring (Supplementary Fig. 2). This arrangement resulted from the in vitro assembly of independently expressed and purified protein components and the existence of two identical KtrB binding surfaces in KtrA.

In the bacterial membrane the KtrAB complex is composed of a homodimeric KtrB membrane protein and a cytoplasmic octameric KtrA ring (Fig.1a). The KtrA octameric ring (Fig. 1a, b and Supplementary Fig. 3) is a four-fold symmetric assembly of four KtrA dimers with the typical RCK domain arrangement[12,13,15], the amino (N) lobe forming the ring and the smaller carboxy (C) lobe at the periphery. The ligand-binding site in the N lobe is occupied by an ATP molecule (Fig. 1a and Supplementary Figs 1b and 3b). The inner circumference of the ring delimits a ~30-Å-wide hole which, together with gaps (approximate dimensions: 17 Å by 9 Å and 18 Å by 11 Å) between the surfaces of the KtrB homodimer and the KtrA ring, give access from the cytosol to the cytoplasmic pore of KtrB (Fig. 1b and Supplementary Fig. 3a).

The interactions between KtrB and the KtrA ring are an important difference relative to K^+ channels[11–15]. In channels the pore subunit and one or two RCK domains are encoded in the same polypeptide and the RCK octameric ring hangs from the cytoplasmic face of the membrane protein through a polypeptide tether. In the KtrAB complex, the KtrB homodimer sits directly on a face of the KtrA ring (Fig. 1c), close to a ring diagonal, and cytoplasmic loops establish two different types of contacts with pairs of RCK domains in the ring: the lateral contact and the tip contact (Fig. 1c, d). The lateral-contact regions involve a mid-section of the KtrB carboxy terminus, which runs along the homodimer interacting with the neighbouring KtrB subunit and the KtrA ring (Fig. 1c, d and Supplementary Fig. 4a). The tip-contact regions occur at the apexes of the cytoplasmic face of the KtrB homodimer (Fig. 1c, d and Supplementary Fig. 4b) where the KtrB cytoplasmic loops connecting repeats D1 and D2 interact with two opposing KtrA subunits. The functional relevance of these interactions and of our *in vitro* assembled KtrAB complex is demonstrated in the Supplementary Discussion.

KtrB structure

The KtrB subunit structure has four repeats (D1 to D4) wrapped around a central axis and cradling the selectivity filter (Figs 1c and 2a). Each repeat (Supplementary Figs 5a, b) includes the M1 helix spanning the bilayer, followed by the P-loop region (that includes the pore (P) helix and the selectivity-filter sequence) and a second shorter (M2a) helix, which ends close to the centre of the membrane. A C-terminal (M2b) helix completes each repeat, running at a shallow angle towards the membrane cytoplasmic face. The selectivity filter is funnel-shaped with its wider mouth (11–13 Å across) towards the extracellular face and the single ion-binding site forming the narrow end (Fig. 2a and Supplementary Fig. 5b). Immediately below the KtrB selectivity filter there is an intramembrane loop (Fig. 2a–c), a residue stretch that connects helices M2a to M2b in repeat D3 and is composed almost exclusively of glycines, alanines and serines (Supplementary Fig. 5c). The intramembrane loop together with a highly conserved arginine (R417) form a structure that blocks access between the selectivity filter and the cytoplasmic pore; mutations or truncations in this region increase ion flux and this region has been proposed to be a transporter gate[9,19]. An open pathway runs from the

INSTITUTO
DE INVESTIGAÇÃO
E INOVAÇÃO
EM SAÚDE
UNIVERSIDADE
DO PORTO

Rua Alfredo Allen, 208
4200-135 Porto
Portugal
+351 220 408 800
info@i3s.up.pt
www.i3s.up.pt

R417/intramembrane loop to the cytoplasmic face of the protein (Fig. 2a). The pathway is lined by a mix of polar and apolar residues and is ~4 Å wide at its narrowest point. Overall, this architecture resembles closely the architecture of potassium channel pores (Supplementary Fig. 6).

The monomer and homodimer structures of KtrB and of the related TrkH[9] (a Trk membrane protein) are very similar (Supplementary Fig. 7). A major difference between KtrB and TrkH is found in the C terminus. In KtrB the long C terminus runs from one subunit, forms a lateral contact and snakes into the cytoplasmic pore of the neighbouring KtrB, finishing just below the intramembrane loop (Figs 1c, d and 2a, b). In contrast, the TrkH C terminus is much shorter and does not establish any contacts (Supplementary Figs 5c and 7a, b). The last seven residues of the KtrB C terminus (Supplementary Fig. 1c) line the wall of the cytoplasmic pore of the neighbouring subunit (Fig. 2a, b). The highly conserved C-terminal glycine (G445) is positioned with its carboxylate interacting with the side chain of a lysine, which is part of the intramembrane loop and is conserved in both the Ktr (K315 in KtrB) and Trk (K357 in TrkH) transporters (Fig. 2c). The C-terminal glycine does not exist in Trk proteins, but in the TrkH structure the side-chain carboxylate of a conserved glutamate (E470) occupies the same volume as the glycine carboxylate and also interacts with the lysine.

To assess the importance of positioning a carboxylate close to the intramembrane loop we generated truncations of the C-terminal residues and evaluated their impact in a growth complementation assay[3,6,8] of the TK2420 *Escherichia coli* strain. This strain has its major K^+ transport systems disabled and only grows in K^+ concentration ≥30 mM; however, when expressing wild-type KtrAB it can grow in K^+ concentrations of ~0.3 mM. The position of the carboxylate does not seem to be essential as sequential truncation of up to three C-terminal residues has no effect or causes only a small shift in rescue (Fig. 2d). Furthermore, the stability of the KtrAB complex seems to be undisturbed (Fig. 2e). However, removal of four residues results in a non-functional transporter, equivalent to control plasmid (Fig. 2d). Consistently, KtrB without the last four residues, although it still forms a homodimer, does not assemble with KtrA (Fig. 2e). All mutations display similar expression levels (Supplementary Fig. 4f). Presumably, the fourth residue, a conserved apolar residue which in the structure seems to function as a C terminus anchor, has a role in the positioning of the C terminus and therefore on the stability of the C-terminus-mediated lateral contact. Notably, we had previously shown that truncation of the last 10 or 15 residues of the C terminus abolishes strain complementation and destabilizes the KtrB dimer[6]. Although we cannot rule out more subtle functional roles for the C terminus, such as cooperativity between KtrB subunits, our results demonstrate that the C terminus has a role both in the stability of the KtrB homodimer and of the KtrAB complex.

Regulation of KtrAB activity

We first determined that KtrA has a strong binding preference for ATP and ADP over other small molecules (Fig. 3a) resembling other KtrA proteins20. The functional effect of these two ligands was then evaluated in a $^{86}Rb^+$ uptake assay[6,9,23] by reconstituting KtrAB with ATP or ADP (Supplementary Fig. 8a) in the presence of an excess of KtrA to minimize the formation of the KtrB–KtrA–KtrB complex. KtrB alone was also reconstituted; it allows K^+ into cells but less efficiently than KtrAB[8].

All protein forms mediate flux in this assay (Fig. 3b). Importantly, flux is markedly higher with ATP, supporting previous cell-based results[20] which showed that ATP is an activator of KtrAB. Noticeably, the $^{86}Rb^+$ flux difference between KtrAB–ATP and KtrB (~2-fold difference at 30 min) is smaller than expected from K^+ uptake measurement in cells[8] (~10-fold difference in

INSTITUTO
DE INVESTIGAÇÃO
E INOVAÇÃO
EM SAÚDE
UNIVERSIDADE
DO PORTO

Rua Alfredo Allen, 208
4200-135 Porto
Portugal
+351 220 408 800
info@i3s.up.pt
www.i3s.up.pt

V_{max}), which may indicate that, in addition to ATP, other activating factors are necessary for full transporter activity.

To understand how the two ligands affect KtrA we determined the crystal structures of this protein bound to ATP and ADP at ~3.2 Å and ,2.9 Å, respectively (Fig. 4a, b and Supplementary Table 1). The ADP- and ATP-bound octameric rings adopt different conformations: the KtrA–ATP ring adopts a four-fold symmetric square conformation and the KtrA–ADP ring adopts a two-fold symmetric diamond conformation. A conformational difference is also observed in solution, through controlled proteolysis (Supplementary Fig. 8b). Both structures present clear electron density for the ligand's adenosine and phosphate groups (Supplementary Fig. 1d, e). Although the conformation of the adenosine group and its interactions with the protein are very similar in the two structures, the phosphate groups are rearranged (Fig. 4c); in particular, the γ-phosphate in the ATP structure occupies the position taken by the β-phosphate in the ADP structure. This is accomplished by a shift in G79 and a repositioning of the α-and β-phosphates relative to the ADP structure. The phosphate–protein interactions are also different: in the ADP structure the β-phosphate interacts with residues from its own binding site, in particular with the side chains R16 and K103; in contrast, in the ATP structure the γ-phosphate interacts with R16 from its binding site, whereas the β-phosphate interacts with R16 from the neighbouring KtrA subunit binding site (Fig. 4c). Presumably owing to the intradimer interactions mediated by ATP, the two binding sites within a KtrA dimer are brought together through a ~16º change in the angle between subunits (Fig. 4d); the distances separating the conserved D36 in the two binding pockets are ~35 Å in the ADP structure and ~30 Å in the ATP structure. This dimer rearrangement is accompanied by rigid-body rotations across two of the four dimer-to-dimer interfaces in the ring and is reflected in the different ring conformations. Most notably the distance separating F71 (a KtrA residue that participates in the KtrAB tip contact region) in opposite ring subunits is 68.7 Å in the KtrA–ATP ring, whereas in KtrA–ADP the equivalent distances are 68.3 and 81.8 Å (Fig.4a,b). Similarly, the distance separating L66 (a KtrA residue that participates in the KtrAB lateral contact region) in KtrA–ATP is 49.8 Å, whereas the equivalent distances in KtrA–ADP are 49.8 and 66.1 Å. Therefore, the conformational change from the KtrA–ADP ring to the ATP ring involves the asymmetric contraction of the ring, with one diagonal direction changing by 13–16 Å, whereas the other diagonal is unaffected.

Notably, the conformation of the octameric ring and the details of ligand binding are basically identical between the isolated KtrA–ATP structure and the KtrA structure that forms the KtrAB–ATP complex (Supplementary Fig. 3a). This suggests that unlike truncated KtrA (composed by N lobe alone; Supplementary Fig. 9) where ligand binding and ring conformation are uncoupled[21], in the full-length KtrA the ATP molecule induces the formation of a unique set of intradimer interactions which determine the conformation of the octameric ring. The absence of the γ-phosphate in ADP is reflected in the lack of ligand-mediated intra-dimer interactions and in the relaxation of the ring.

Implications for KtrAB activation

We have uncovered several differences between KtrAB and the BK[13–15] and MthK[11,12,24] channels which have an impact on their mechanisms of transport activation. In channels, the RCK rings are covalently tethered to the C terminus of a single channel pore domain and the rings expand symmetrically upon binding of an activating ligand. In KtrAB, the cytoplasmic loops of the KtrB homodimer mediate the interaction with the KtrA (RCK) ring and the ring contracts asymmetrically upon binding of ATP.

To propose an activation mechanism for KtrAB we need to define its 'gates' (that is, regions that undergo a conformational change and close/open the ion pathway)—ion transporters[25] and

INSTITUTO
DE INVESTIGAÇÃO
E INOVAÇÃO
EM SAÚDE
UNIVERSIDADE
DO PORTO

Rua Alfredo Allen, 208
4200-135 Porto
Portugal
+351 220 408 800
info@i3s.up.pt
www.i3s.up.pt

channels[26] can have multiple gates. In KtrAB, the intramembrane loop has been proposed to be a gate[9,19]. A comparison between KtrB and TrkH structures (Supplementary Fig. 7a–d) raises the possibility of another gate region; it shows the M2b helix/D1–D2 loop region adopting different conformations. In TrkH, helices M2a and M2b (in repeat D1) are continuous and the ordered amino acid stretch of the D1–D2 loop is positioned so that it partially obstructs the cytoplasmic ion pathway of KtrB. This indicates that this region is able to adopt different positions and could function as a gate.

We foresee therefore two possible activation mechanisms for KtrAB (see also Supplementary Discussion[27,28]). For model 1, the asymmetric KtrA contraction/expansion occurs along the diagonal defined by the lateral contacts (Fig. 5a, b). The direct connection between the KtrB C terminus, involved in the lateral-contact region, and the R417/intramembrane loop gate suggests that this would be the KtrA controlled gate. There are two pieces of evidence against this model: first, the R417/intramembrane gate seems to be closed in the KtrAB structure bound to ATP, an activating ligand. Second, sequential truncations of 1–3 residues in the C terminus have no apparent functional consequence. For model 2, the asymmetric change in KtrA occurs along the diagonal defined by the tip contacts (Fig. 5a, c). We see no obvious direct structural link between the tip-contact region, formed by the D1–D2 loop in KtrB, and the R417/intramembrane gate (Fig. 2a). A clear alternative is that the D1–D2 loop is the KtrA controlled gate, whereas the R417/intramembrane gate is activated by an as-yet-unknown stimulus. Upon ATP binding, the D1–D2 loop would adopt the conformation seen in the KtrAB structure, opening the cytoplasmic pore and resulting in an increase in transporter activity, as detected by our functional assay. Full transporter activity, as seen in cells[8], would require not just ATP but also the influence of another stimulus to activate the intramembrane gate.

In summary, this study provides novel insights and raises new ideas about the structure and mechanism of regulation of the KtrAB K^+ transporter, offering a better understanding of the function of the Trk/Ktr/HKT transporters in bacteria, archaea, fungi and plants.

METHODS SUMMARY

Briefly, *B. subtilis* KtrB was overexpressed in the BL21(DE3) *E. coli* strain, protein extracted with dodecylmaltoside, affinity purified in cobalt matrix and further purified by size-exclusion chromatography. Tag-less *B. subtilis* KtrA protein was overexpressed in BL21(DE3), and protein was purified by affinity chromatography in an ADP-agarose matrix. KtrAB complex was assembled by mixing KtrB and KtrA. Preparation of proteoliposomes and $^{86}Rb^+$ flux assay was performed as previously described with some variations[6,29]. For crystallization the complex was further purified and detergent exchanged to Cymal6 by size-exclusion chromatography. Structure determination and representation made use of XDS[30], MOSFLM[31], PHYRE[32], PHASER[33], PHENIX[34], RAVE[35], COOT[36], Diffraction Anisotropy Server[37], PYMOL[38], STRAP[39], ESPrit[40], Hollow[41] and CCP4[42] programs. Growth complementation assay followed protocols previously described[6,8]. Protein quality control was performed by mass spectrometry.

REFERENCES

1. Corratgé-Faillie, C. et al. Potassium and sodium transport in non-animal cells: the Trk/Ktr/HKT transporter family. Cell. Mol. Life Sci. 67, 2511–2532 (2010).

2. Durell, S. R., Hao, Y., Nakamura, T., Bakker, E. P. & Guy, H. R. Evolutionary relationship between K^+ channels and symporters. Biophys. J. 77, 775–788 (1999).

3. Nakamura, T., Yuda, R., Unemoto, T. & Bakker, E. P. KtrAB, a new type of bacterial K^+-uptake system from *Vibrio alginolyticus*. J. Bacteriol. 180, 3491–3494 (1998).

INSTITUTO
DE INVESTIGAÇÃO
E INOVAÇÃO
EM SAÚDE
UNIVERSIDADE
DO PORTO

Rua Alfredo Allen, 208
4200-135 Porto
Portugal
+351 220 408 800
info@i3s.up.pt
www.i3s.up.pt

4. Hänelt, I. et al. KtrB, a member of the superfamily of K^+ transporters. Eur. J. Cell Biol. 90, 696–704 (2011).

5. Tholema, N., Bakker, E. P., Suzuki, A. & Nakamura, T. Change to alanine of one out of four selectivity filter glycines in KtrB causes a two orders of magnitude decrease in the affinities for both K^+ and Na^+ of the Na^+ dependent K^+ uptake system KtrAB from *Vibrio alginolyticus*. FEBS Lett. 450, 217–220 (1999).

6. Albright, R. A., Joh, K. & Morais-Cabral, J. H. Probing the structure of the dimeric KtrB membrane protein. J. Biol. Chem. 282, 35046–35055 (2007).

7. Maser, P. et al. Glycine residues in potassium channel-like selectivity filters determine potassium selectivity in four-loop-per-subunit HKT transporters from plants. Proc. Natl Acad. Sci. USA 99, 6428–6433 (2002).

8. Tholema, N. et al. All four putative selectivity filter glycine residues in KtrB are essential for high affinity and selective K^+ uptake by the KtrAB system from *Vibrio alginolyticus*. J. Biol. Chem. 280, 41146–41154 (2005).

9. Cao, Y. et al. Crystal structure of a potassium ion transporter, TrkH. Nature 471, 336–340 (2011).

10. Doyle, D. A. et al. The structure of the potassium channel: molecular basis of K^+ conduction and selectivity. Science 280, 69–77 (1998).

11. Jiang, Y. et al. The open pore conformation of potassium channels. Nature 417, 523–526 (2002).

12. Jiang, Y. et al. Crystal structure and mechanism of a calcium-gated potassium channel. Nature 417, 515–522 (2002).

13. Wu, Y., Yang, Y., Ye, S. & Jiang, Y. Structure of the gating ring from the human large-conductance Ca^{2+}-gated K^+ channel. Nature 466, 393–397 (2010).

14. Yuan, P., Leonetti, M. D., Pico, A. R., Hsiung, Y. & MacKinnon, R. Structure of the human BK channel Ca^{2+}-activation apparatus at 3.0 Å resolution. Science 329, 182–186 (2010).

15. Yuan, P., Leonetti, M. D., Hsiung, Y. & MacKinnon, R. Open structure of the Ca^{2+} gating ring in the high-conductance Ca^{2+}-activated K^+ channel. Nature 481, 94–97 (2012).

16. Holtmann, G., Bakker, E. P., Uozumi, N. & Bremer, E. KtrAB and KtrCD: two K^+ uptake systems in *Bacillus subtilis* and their role in adaptation to hypertonicity. J. Bacteriol. 185, 1289–1298 (2003).

17. Berry, S. et al. Potassium uptake in the unicellular cyanobacterium *Synechocystis* sp. strain PCC 6803 mainly depends on a Ktr-like system encoded by slr1509 (ntpJ). FEBS Lett. 548, 53–58 (2003).

18. Matsuda, N. et al. Na^+-dependent K^+ uptake Ktr system from the cyanobacterium Synechocystis sp. PCC 6803 and its role in the early phases of cell adaptation to hyperosmotic shock. J. Biol. Chem. 279, 54952–54962 (2004).

19. Hanelt, I. et al. Gain of function mutations in membrane region M2C2 of KtrB open a gate controlling K^+ transport by the KtrAB system from *Vibrio alginolyticus*. J. Biol. Chem. 285, 10318–10327 (2010).

20. Kroning, N. et al. ATP binding to the KTN/RCK subunit KtrA from the K^+-uptake system KtrAB of *Vibrio alginolyticus*: its role in the formation of the KtrAB complex and its requirement *in vivo*. J. Biol. Chem. 282, 14018–14027 (2007).

21. Albright, R. A., Ibar, J. L., Kim, C. U., Gruner, S. M. & Morais-Cabral, J. H. The RCK domain of the KtrAB K^+ transporter: multiple conformations of an octameric ring. Cell 126, 1147–1159 (2006).

INSTITUTO
DE INVESTIGAÇÃO
E INOVAÇÃO
EM SAÚDE
UNIVERSIDADE
DO PORTO

Rua Alfredo Allen, 208
4200-135 Porto
Portugal
+351 220 408 800
info@i3s.up.pt
www.i3s.up.pt

22. Roosild, T. P., Miller, S., Booth, I. R. & Choe, S. A mechanism of regulating transmembrane potassium flux through a ligand-mediated conformational switch. Cell 109, 781–791 (2002).

23. Heginbotham, L., Kolmakova-Partensky, L. & Miller, C. Functional reconstitution of a prokaryotic K^+ channel. J. Gen. Physiol. 111, 741–749 (1998).

24. Ye, S., Li, Y., Chen, L. & Jiang, Y. Crystal structures of a ligand-free MthK gating ring: insights into the ligand gating mechanism of K^+ channels. Cell 126, 1161–1173 (2006).

25. Olesen, C. et al. The structural basis of calcium transport by the calcium pump. Nature 450, 1036–1042 (2007).

26. Cuello, L. G. et al. Structural basis for the coupling between activation and inactivation gates in K^+ channels. Nature 466, 272–275 (2010).

27. Trudeau, M. C. Unlocking the mechanisms of HCN channel gating with locked-open and locked-closed channels. J. Gen. Physiol. 140, 457–461 (2012).

28. Hilf, R. J. & Dutzler, R. A prokaryotic perspective on pentameric ligand-gated ion channel structure. Curr. Opin. Struct. Biol. 19, 418–424 (2009).

29. Nimigean, C. M. A radioactive uptake assay to measure ion transport across ion channel-containing liposomes. Nature Protocols 1, 1207–1212 (2006).

30. Kabsch, W. Xds. Acta Crystallogr. D 66, 125–132 (2010).

31. Leslie, A. G. The integration of macromolecular diffraction data. Acta Crystallogr. D 62, 48–57 (2006).

32. Kelley, L. A. & Sternberg, M. J. Protein structure prediction on the Web: a case study using the Phyre server. Nature Protocols 4, 363–371 (2009).

33. McCoy, A. J. et al. Phaser crystallographic software. J. Appl. Crystallogr. 40, 658–674 (2007).

34. Adams, P. D. et al. PHENIX: a comprehensive Python-based system for macromolecular structure solution. Acta Crystallogr. D 66, 213–221 (2010).

35. Kleywegt, G. J. & Jones, T. A. Software for handling macromolecular envelopes. Acta Crystallogr. D 55, 941–944 (1999).

36. Emsley, P. & Cowtan, K. Coot: model-building tools for molecular graphics. Acta Crystallogr. D 60, 2126–2132 (2004).

37. Strong, M. et al. Toward the structural genomics of complexes: crystal structure of a PE/PPE protein complex from Mycobacterium tuberculosis. Proc. Natl Acad. Sci. USA 103, 8060–8065 (2006).

38. Schrodinger, LLC. The PyMOL Molecular Graphics System, Version 1.3r1(2010).

39. Gille, C. & Frommel, C. STRAP: editor for STRuctural Alignments of Proteins. Bioinformatics 17, 377–378 (2001).

40. Gouet, P., Robert, X. & Courcelle, E. ESPript/ENDscript: Extracting and rendering sequence and 3D information from atomic structures of proteins. Nucleic Acids Res. 31, 3320–3323 (2003).

41. Ho, B. K. & Gruswitz, F. HOLLOW: generating accurate representations of channel and interior surfaces in molecular structures. BMC Struct. Biol. 8, 49 (2008).

42. Winn, M. D. et al. Overview of the CCP4 suite and current developments. Acta Crystallogr. D 67, 235–242 (2011).

Acknowledgements We are grateful for access to ID14-1/ID14-4/ID-29 at ESRF (through the Portuguese BAG), PXII at SLS, XRD1 at ELETTRA and PROXIMA1 at SOLEIL and thank the respective

support staff. A.S. was supported by FEBS (Long term fellowship). This work was funded by EMBO (Installation grant), by FEDER funds through the Operational Competitiveness Program–COMPETE and by National Funds through FCT–Fundação para a Ciência e a Tecnologia under the projects FCOMP-01-0124-FEDER-022718 (PEst-C/SAU/LA0002/2011), FCOMP-01-0124-FEDER-009028 (PTDC/BIA-PRO/099861/2008) and FCOMP-01-0124-FEDER-010781 (PTDC/QUI-BIQ/105342/2008). We also thank G. Gabant and M. Cadene at the 'Plateforme de Spectrometrie de Masse' at CBM, CNRS, Orleans for mass spectrometry analysis, and C. Harley for critical reading of the manuscript.

Author Contributions R.S.V.-P. performed all crystallographic work with the support of J.H.M.-C.;R.S.V.-P.andA.S.performedthefunctionalandbiochemicalcharacterization; J.H.M.-C., R.S.V.-P. and A.S. designed experiments and wrote the manuscript.

Author Information Structures have been deposited in the Protein Data Bank under accessions 4J7C (KtrAB complex), 4J90 (KtrA–ATP) and 4J91 (KtrA–ADP). Reprints and permissions information is available at www.nature.com/reprints. The authors declare no competing financial interests. Readers are welcome to comment on the online version of the paper. Correspondence and requests for materials should be addressed to J.H.M.-C. (jcabral@ibmc.up.pt).

METHODS

Protein expression and purification. N-terminal His-tagged KtrB was overexpressed in *E. coli* BL21 (DE3), in LB media at 37uC for 2.5 h after IPTG induction. After cell lysis in Buffer A (50 mM Tris-HCl pH 8.0, 120 mM NaCl, 30 mM KCl) supplemented with protease inhibitors, the lysate was supplemented with 40 mM DDM (*n*-dodecyl-β-D-maltoside, solgrade from Anatrace) for membrane protein extraction overnight at 4 ºC. Spin-cleared lysate was loaded onto a Talon metal affinity resin (Clontech) and washed with Buffer B (50 mM Tris-HCl pH 8.0, 120 mM NaCl, 30 mM KCl, 1 mM DDM). Protein was eluted with Buffer B supplemented with 150 mM imidazole. Eluted fractions were concentrated to ~2.5 mg ml^{-1} and incubated overnight at 4 ºC with thrombin for tag cleavage. At this point the protein was either directly used for KtrAB complex assembly or further purified by size exclusion with a Superdex-200 column.

Tag-less KtrA was overexpressed in *E. coli* BL21 (DE3), in LB media at 20 ºC for 14–16 h after IPTG induction. Cells lysis was done in Buffer C (50 mM Tris-HCl pH 7.5, 50 mM KCl, 5 mM DTT) and cleared lysate loaded into an anion exchange column. Fractions containing KtrA were incubated with ADP-agarose resin (Innova Biosciences) overnight at 4 ºC. Beads were washed thoroughly with Buffer D (50 mM Tris-HCl, 150 mM KCl, 1 mM TCEP) and protein was eluted in the same buffer supplemented with 5 mM of adenosine-containing nucleotide. At this point the protein was concentrated to ~3 mg ml^{-1} and either directly used for KtrAB complex assembly or further purified by size exclusion with a Superdex-S200 column.

KtrAB complex was assembled by mixing individually purified KtrB and KtrA batches, at a pre-defined ratio. The complex mixture was further concentrated (~20 mg ml^{-1}) and purified in a size-exclusion Superdex-200 column with Buffer E (20 mM Tris-HCl pH 8.0, 120 mM NaCl, 30 mM KCl, 5 mM DTT, 1.5 mM 6-cyclohexyl-1-hexyl-β-D-maltoside (cymal-6, anagrade from Anatrace)).

Crystallization. KtrAB complex purified in Buffer E supplemented with 1 mM ATP (ATP) was concentrated to ~10mg ml^{-1} and dialysed overnight against the same buffer before crystallization assays. KtrAB complex crystals were obtained by the sitting-drop vapour diffusion method, mixing 1 µl of protein with 1 µl of crystallization solution. The best diffracting crystals grew in 100 mM *N*-(2-acetamido)-iminodiacetic acid (ADA) pH 6.5, 20% polyethylene glycol 400 (PEG 400) and 200 mM ammonium sulphate at 20 ºC. Crystals were flash-frozen in liquid nitrogen after addition of mother liquor with 45% PEG 400 directly to the crystal drop.

Before crystallization KtrA–ATP and KtrA–ADP were run in a size-exclusion chromatography column equilibrated with Buffer F (50 mM Tris-HCl pH 7.5, 150 mM KCl, 5 mM DTT, 1 mM ATP or ADP). KtrA–ATP crystals were grown by sitting-drop vapour diffusion with 100 mM HEPES pH 7.5, 3% polyethylene glycol 6000 (PEG 6000) and 2.5% 2-methyl-2,4-pentanediol (MPD) at 20 ºC. Crystals were flash frozen in liquid nitrogen after being transferred to identical mother liquor containing 6% PEG 6000 and 30% glycerol. KtrA–ADP crystals were obtained with 100 mM citrate pH 5.6, 14.5% PEG 2000 and 200 mM ammonium sulphate at 20 ºC. Crystals were flash-frozen in liquid nitrogen after addition of modified mother liquor, with 15% PEG 2000 and 20% glycerol, directly to the crystal drop.

INSTITUTO
DE INVESTIGAÇÃO
E INOVAÇÃO
EM SAÚDE
UNIVERSIDADE
DO PORTO

Rua Alfredo Allen, 208
4200-135 Porto
Portugal
+351 220 408 800
info@i3s.up.pt
www.i3s.up.pt

Data processing and structure determination. Diffraction data were processed with XDS[30] or MOSFLM[31], followed by scaling with CCP4 package[42]. Data from KtrAB crystals is highly anisotropic and was analysed, truncated and sharpened in the Diffraction Anisotropy Server[37] (http://services.mbi.ucla.edu/anisoscale/). Recommended resolution limits after anisotropic correction were 3.8 Å, 4.1 Å and 3.3 Å, respectively, along the a^*, b^* and c^* reciprocal space directions.

KtrA–ATP structure was determined by molecular replacement with PHASER[33] using as search models the truncated KtrA N-lobe structure (Protein Data Bank code 2HMU) and C-lobe homology models generated by PHYRE[32]. Improvement of electron-density maps, in particular on the C-lobe region, was achieved by cross-crystal averaging between KtrA–ATP and truncated KtrA using MAMA[35] and DMmulti (CCP4 package). The structure was finalized with cycles of model building with COOT[36] and refinement with PHENIX[34] and REFMAC (CCP4 package). The two subunits in the asymmetric unit include residues 6 to 222. Ramachandran plot for KtrA–ATP structure contains: 0% outliers, 1.63% allowed, 98.37% preferred.

The N and C lobes of KtrA–ATP structure were used for molecular replacement with the KtrA–ADP data. Cycles of averaging between the four subunits of KtrA–ADP and the two subunits of KtrA–ATP improved maps. Model building and refinement produced a final model of KtrA–ADP that includes: in chain A, residues 8–157, 162–174 (built as alanines), 177–222; in chain B, residues 8–222; in chain C, residues 8–147, 152–157,161–176 (built as alanines), 177–222; in chain D, residues 8–187, 188–192 (built as alanines), 196–222. Ramachandran plot for KtrA–ADP structure contains: 0% outliers, 1.82% allowed, 98.18% preferred.

The KtrAB structure was determined by molecular replacement using as search models a poly-alanine version of the TrkH dimer structure (Protein Data Bank code 3PJZ) and the KtrA–ATP octameric ring structure. Cycles of four-fold averaging for the KtrB subunits and eight-fold averaging for the KtrA ring subunits together with cross-crystal averaging with the KtrA–ATP structure resulted in great improvements in the electron-density maps and allowed tracing of the KtrB chain. Chain trace was confirmed with a selenomethionine anomalous map calculated to 7.4 Å, which at a 3.6s contour revealed the position of 9 methionines out of 14 possible (Supplementary Fig. 10), and through a comparison with the TrkH structure. Structure was finalized through cycles of model building and refinement. The model was refined against data to 3.5 Å as there was no visible improvement in refinement statistics or map quality with data to the recommended limit (see above). In the KtrAB structure the KtrB subunits span residues 15 to 445 (except for a missing stretch formed by residues 103 and 104) whereas the KtrA subunits span residues 7–222. Ramachandran plot for KtrAB crystals: 0% outliers, 5.94% allowed, 94.06% preferred. Model analysis was performed with PYMOL[38], STRAP[39], ESPrit[40] and Hollow[41].

Complementation assay. The complementation assay with TK2420 follows procedures previously described[3,6,8]. Briefly, mutants and wild-type KtrB and KtrA were cloned into a dicistronic constitutive expression plasmid. The TK2420 strain was transformed with the different plasmids and plated on LBK (Luria–Bertani broth where NaCl is replaced by KCl) agar plates. Single colonies were picked and grown in liquid LBK overnight at 37 ºC. A 2-ml aliquot of cells was gently pelleted and re-suspended in 400 µl of minimal media containing 0.1 mM K^+. A 15 µl aliquot of re-suspended cells was then used to inoculate 5 ml of minimal media prepared with different K^+ concentrations (0.1, 0.3, 1, 2, 6, 10, 30 or 115 mM) and grown for 15 h at 37 ºC at which point optical density at 595 nm was measured.

Preparation of proteoliposomes. Preparation follows previously described methods[6,29]. Polar *E. coli* lipids in chloroform were dried under a stream of argon, washed in pentane and dried again. Residual solvent was removed under vacuum. Lipids were re-suspended at 10 mg ml^{-1} in swelling buffer (150 mM KCl, 10 mM HEPES, 5 mM *N*-methylglucamine, pH 7.6) using a bath sonicator. Lipids were solubilized by adding decylmaltoside (powder) to 40 mM. After 2 h of gentle agitation, dodecylmaltoside-solubilized protein, in KtrB buffer (150 mM KCl, 20 mM Tris-HCl, 5 mM DTT, 0.5 mM dodecylmaltoside, 200 µM NTP, pH 8.0), was added at 1:100 w:w protein-to-lipid ratio and incubated for 30 min at room temperature. KtrAB complex was assembled just before reconstitution with excess of either ATP-bound KtrA or ADP-bound KtrA. The amount of protein added to 100 µl solubilized lipids was adjusted to contain 10 µg KtrB both when reconstituted alone or as KtrAB complex. Detergent was removed by dialysis against swelling buffer supplemented with 20 µM ATP or ADP and with Na^+ concentration at 40 µM, using 15 kDa cutoff dialysis membranes for 4 days at 4 ºC. Control liposomes were prepared similarly, except that only KtrA was added to the solubilized lipids.

$^{86}Rb^+$ flux assay. Assay as previously described[6,29],with small modifications. A gradient of K^+ across the liposome membrane was generated, immediately before the assay, by loading 100 µl aliquot of liposomes into a 5 ml disposable spin column containing Sephadex G50 (fine) pre-swollen with sorbitol buffer (20 µM KCl, 150 mM sorbitol, 10 mM HEPES, 5 mM *N*-methylglucamine, pH 7.6) and centrifuging for 1 min at 700*g*. After forming the gradient, liposomes were supplemented with 20 µM ADP or ATP (final concentration of Na+ was set to 40 µM) and mixed with three volume of $^{86}Rb^+$ assay buffer ($^{86}Rb^+$ at ~2,000 counts μl^{-1} in sorbitol buffer). At different time points 100 µl of uptake reaction were loaded on a 1.5-ml bed volume Dowex cation exchange columns (pre-washed in 150mM sorbitol solution plus 5 mg ml^{-1} BSA to avoid unspecific binding to resin, and then pre-equilibrated in 150 mM sorbitol solution) and eluted with 6% sorbitol solution. The eluate was collected in 4-ml scintillation vials and mixed with 1.5 ml Optiphase scintillation fluid. At the end of the experiment 900 nM valinomycin was added to the last 100 µl aliquot of the uptake reaction, incubated for 3 min and then loaded on Dowex columns as described above. The uptake of $^{86}Rb^+$ into liposomes was expressed as the percentage of the counts measured after valinomycin treatment (this provides a correction for the internal volume of liposomes in the reaction sample). Valinomycin was also applied at earlier time points to check whether the long timescale of the experiments could affect the final counts, but the values were similar to those measured after 2 h. For all conditions means 6 s.e.m. of triplicates were calculated for two separate liposome preparations.

KtrA ligand binding. Potential ligands for KtrA were screened by making use of the tight binding of isolated KtrA to an ADP-agarose matrix and by evaluating which small molecules elute the protein from the beads. Purified KtrA was incubated with the beads at 4 ºC. Beads were washed with buffer and then incubated for 30 min with 1 mM of different ligands: ATP (adenosine triphosphate), ADP (adenosine diphosphate), AMP (adenoside monophosphate), FAD (flavin mononucleotide), NAD (nicotinamide adenine dinucleotide), NADH (reduced NAD), NADPH (reduced nicotinamide adenine dinucleotide phosphate) and GTP (guanosine triphosphate). Eluted fractions were run in an SDS–PAGE.

INSTITUTO
DE INVESTIGAÇÃO
E INOVAÇÃO
EM SAÚDE
UNIVERSIDADE
DO PORTO

Rua Alfredo Allen, 208
4200-135 Porto
Portugal
+351 220 408 800
info@i3s.up.pt
www.i3s.up.pt

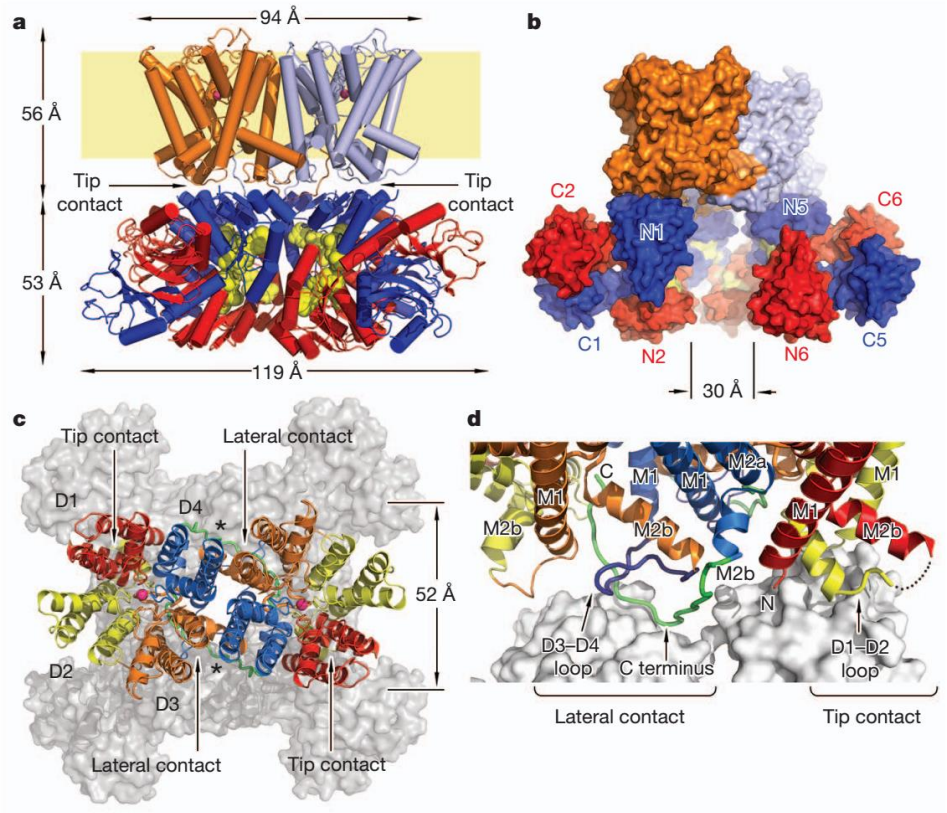

Figure 1 | Structure of the KtrAB K^+ transporter. a, Cartoon of the KtrAB structure with the extracellular side at the top. KtrB subunits are in orange and light blue whereas KtrA subunits are in dark blue and red; ATP is shown as yellow spheres and K^+ as magenta spheres; cell membrane is shown as a pale yellow rectangle. **b,** Surface representation of KtrAB rotated relative to panel a along the vertical axis. One KtrA dimer has been removed for viewing the hole at centre of the octameric ring. N and C lobes of KtrA subunits are indicated. **c,** Extracellular view of KtrB repeats (D1, red; D2, yellow; D3, orange; D4, blue); KtrA is shown as grey surface. Asterisks indicate green KtrB C termini running along the KtrB dimer. **d,** Detail of contact regions. Colouring as in panel c except for the D3–D4 loop, shown in purple. The disordered stretch in the D1–D2 loop is shown as a dotted line. KtrB helices and N and C termini are labelled.

INSTITUTO DE INVESTIGAÇÃO E INOVAÇÃO EM SAÚDE
UNIVERSIDADE DO PORTO

Rua Alfredo Allen, 208
4200-135 Porto
Portugal
+351 220 408 800
info@i3s.up.pt
www.i3s.up.pt

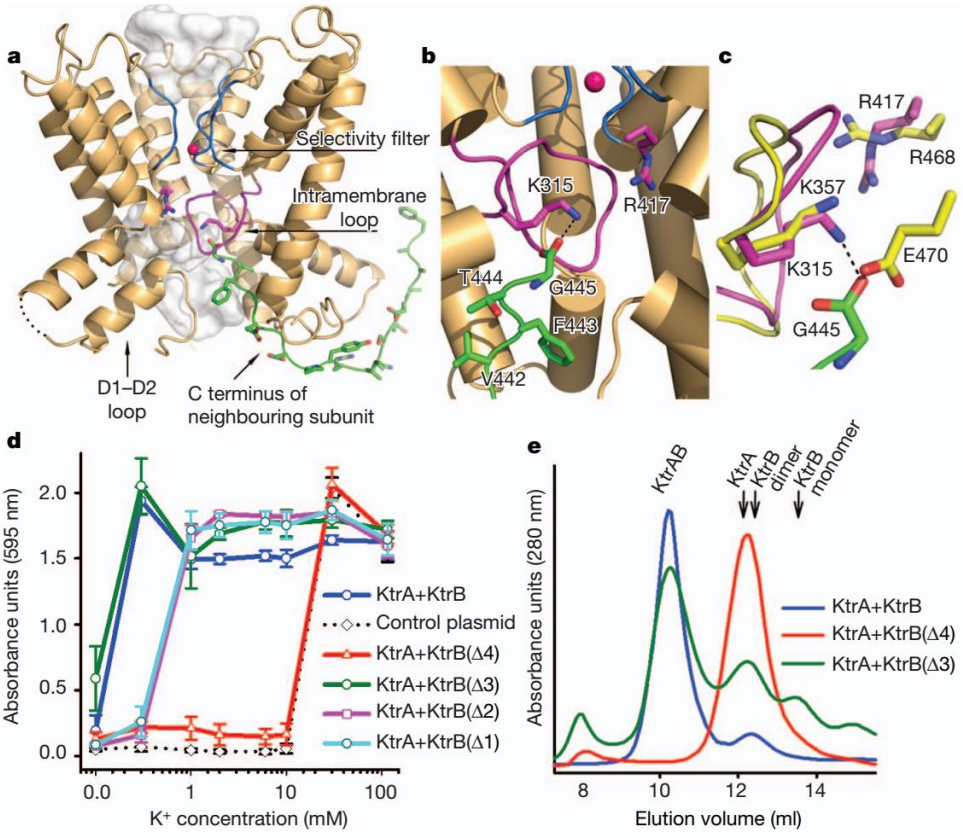

Figure 2 | KtrB subunit. a, KtrB subunit without repeat D2. K^+ ion is indicated as a red sphere; the intramembrane loop, K315 (at the centre) and R417 (on the left) are shown in magenta. The ion pathway, calculated with Hollow[41] with a 1.4 Å probe radius, is shown as a white surface. **b,** Close-up view of ion pathway, rotated 180º relative to panel **a.** C-terminal residues from the neighbouring KtrB subunit are shown in green stick representation. **c,** Intramembrane loops in KtrB (magenta and green) and TrkH (yellow), after superposition of pore regions. **d,** Optical density of *E. coli* TK2420 (expressing different constructs) cultures versus K^+ concentration. Δ1, Δ2, Δ3 and Δ4 indicate KtrB C-terminal sequential truncations. Mean ± s.d. from three independent experiments is shown. **e,** Size-exclusion chromatography elution profiles of mixtures of wild-type KtrA and wild-type or mutant KtrB, at same concentrations and ratios. Elution volumes for KtrAB, KtrA (octamer) and KtrB (monomer and dimer) are indicated.

INSTITUTO DE INVESTIGAÇÃO E INOVAÇÃO EM SAÚDE
UNIVERSIDADE DO PORTO

Rua Alfredo Allen, 208
4200-135 Porto
Portugal
+351 220 408 800
info@i3s.up.pt
www.i3s.up.pt

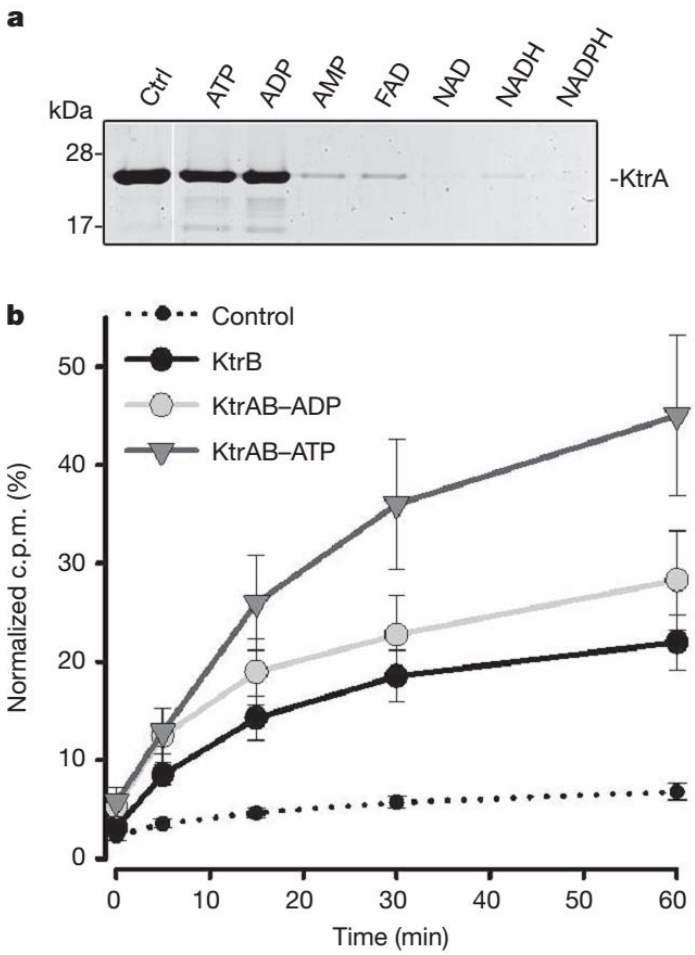

Figure 3 | Ligand regulation of KtrAB transporter. a, SDS–PAGE of KtrA protein eluted from ADP-agarose with 1 mM of different adenosine-containing ligands. Purified KtrA is indicated as Ctrl. **b,** Time course of normalized $^{86}Rb^{+}$ uptake into liposomes with reconstituted KtrAB transporter (with ATP or ADP) or KtrB alone (with ATP). Control measurement was with liposomes formed in the presence of KtrA alone; normalization after addition of valinomycin at end of assay. Mean ± s.e.m. calculated from six assays corresponding to triplicates from two separate liposome preparations. c.p.m., counts per minute.

INSTITUTO
DE INVESTIGAÇÃO
E INOVAÇÃO
EM SAÚDE
UNIVERSIDADE
DO PORTO

Rua Alfredo Allen, 208
4200-135 Porto
Portugal
+351 220 408 800
info@i3s.up.pt
www.i3s.up.pt

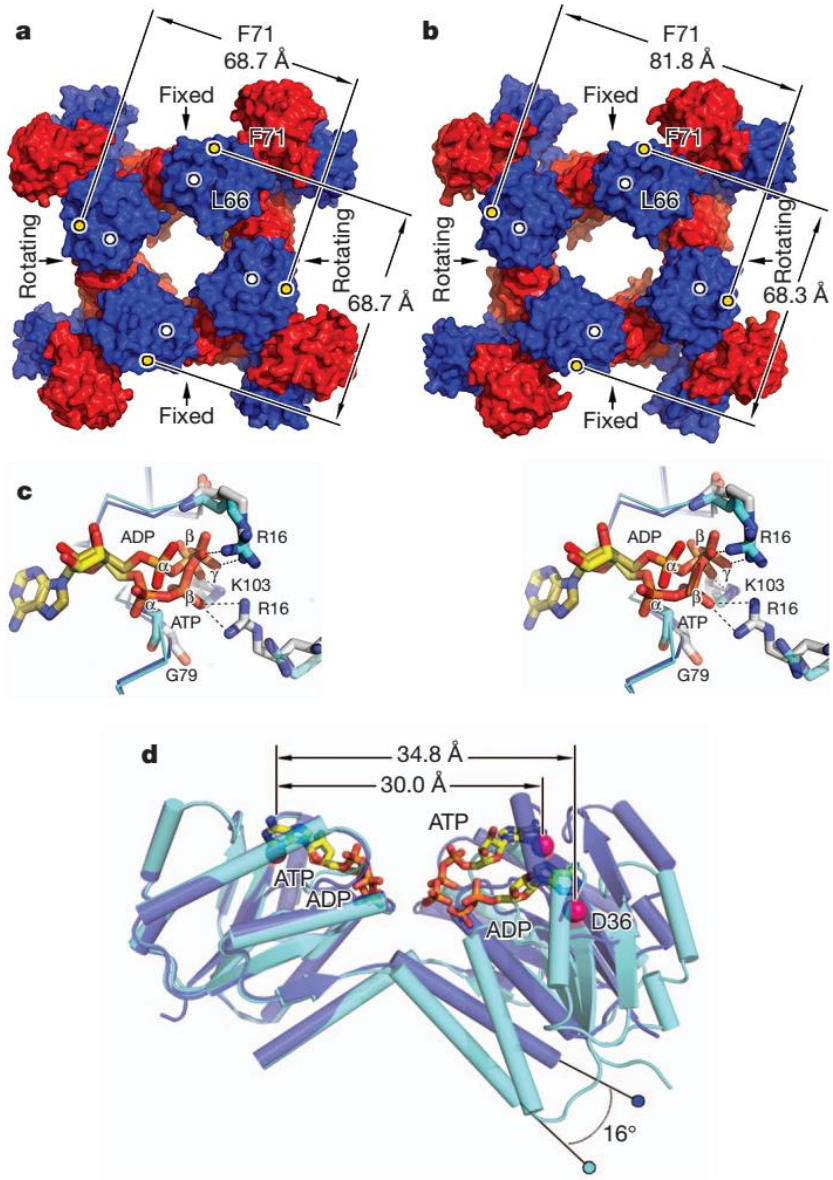

Figure 4 | Conformational changes in the KtrA octameric ring. a, b, Surface representations of isolated KtrA–ATP ring (**a**) and KtrA–ADP ring (**b**). KtrA subunits are shown in red and blue. F71 Ca is shown as yellow dots; L66 Ca is shown as white dots. Dimer-to-dimer interfaces that undergo a rigid-body rotation between ATP- and ADP-bound states are indicated as rotating; the other dimer-to-dimer interfaces are indicated as fixed. **c,** Stereo view of superposed ligand-binding sites from KtrA–ADP (light blue Cα trace and side-chain stick) and KtrA–ATP (dark blue Cα trace and white side-chain stick). Residues, ATP and ADP molecules and ligand phosphates are labelled. Some ligand–protein interactions are shown as dashed lines. **d,** Superposition of a KtrA–ATP (dark blue) and KtrA–ADP (light blue) dimer through one of the subunits; only N lobes are shown. Ligands are shown as stick representation. The distance separating D36 residues (red spheres) in dimer subunits and dimer hinge angle change are indicated.

INSTITUTO
DE INVESTIGAÇÃO
E INOVAÇÃO
EM SAÚDE
UNIVERSIDADE
DO PORTO

Rua Alfredo Allen, 208
4200-135 Porto
Portugal
+351 220 408 800
info@i3s.up.pt
www.i3s.up.pt

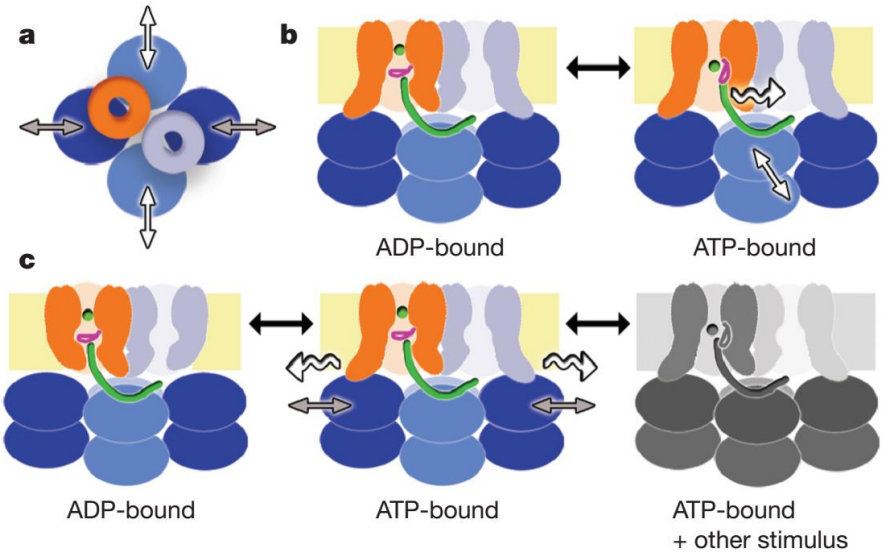

Figure 5 | Models for KtrAB activation. Cartoon with the KtrB homodimer in orange and grey; KtrA subunits as dark- and light-blue ovals; intramembrane loop in magenta; C terminus as green coil; and K^+ as green sphere. **a,** Extracellular view with asymmetric conformational changes in the KtrA ring occurring along two possible directions: along lateral contact (pair of white arrows) or along tip contact (grey arrows). **b, c,** Side views of KtrAB. For model 1 (**b**), KtrA asymmetrical conformational change along lateral contact is propagated through the KtrB C terminus to intramembrane loop gate (indicated by wavy arrow). For model 2 (**c**), KtrA asymmetrical conformational change along tip contact alters conformation of the KtrB D1–D2 loop gate (wavy arrows), opening a gate. For full activation the intramembrane loop gate has to open upon an as-yet-unknown stimulus (cartoon representation in dark grey).

INSTITUTO
DE INVESTIGAÇÃO
E INOVAÇÃO
EM SAÚDE
UNIVERSIDADE
DO PORTO

Rua Alfredo Allen, 208
4200-135 Porto
Portugal
+351 220 408 800
info@i3s.up.pt
www.i3s.up.pt